Research Square

Preprints are preliminary reports that have not undergone peer review.
They should not be considered conclusive, used to inform clinical practice,
or referenced by the media as validated information.

LEFM-Based Evaluation of Structural Stress Approaches for Fatigue Assessment of Welded CHS with Large Geometric Scale Differences

Stefan Vogts

stefan.vogts@tu-braunschweig.de

TU Braunschweig: Technische Universitat Braunschweig https://orcid.org/0009-0008-2628-5143

Jörg Baumgartner

Fraunhofer-Institut fur Betriebsfestigkeit und Systemzuverlassigkeit LBF

Julian Unglaub

TU Braunschweig: Technische Universitat Braunschweig

Klaus Thiele

TU Braunschweig: Technische Universitat Braunschweig

Research Article

Keywords: Finite Element Analysis, Structural Stress, Circular Hollow Sections, Fatigue, Design of Experiments, Linear Elastic Fracture Mechanics

Posted Date: November 6th, 2026

DOI: https://doi.org/10.21203/rs.3.rs-11376797/v1

License: This work is licensed under a Creative Commons Attribution 4.0 International License.
Read Full License

LEFM-Based Evaluation of Structural Stress Approaches for Fatigue Assessment of Welded CHS with Large Geometric Scale Differences

Stefan Vogts[1*], Jörg Baumgartner[2], Julian Unglaub[1], Klaus Thiele[1]

[1*]Institute of Steel Structures, Technische Universität Braunschweig, Beethovenstr. 51, Braunschweig, 38106, Lower Saxony, Germany.
[2]Research and Development, Fraunhofer Institute for Structural Durability and System Reliability LBF, Bartningstr. 47, Darmstadt, 64289, Hessen, Germany.

*Corresponding author(s). E-mail(s): stefan.vogts@tu-braunschweig.de;

Abstract

Fatigue assessment of welded offshore structures commonly relies on hot-spot stress (HSS) approaches. However, pronounced geometric scale differences between monopile shells and welded secondary attachments, such as boat landings, may place these joints outside the applicability ranges of established tubular-joint recommendations. This study compares five structural stress approaches for single-sided welded circular hollow section (CHS) joints: IIW plate extrapolation, IIW/CIDECT and DNV-RP-C203 tubular-joint extrapolation, the Xiao–Yamada (XY) 1 mm stress approach, and Dong's structural stress method. Chord-side stress concentration factors (SCFs) were determined using linear-elastic finite-element analyses within a Design of Experiments (DoE) framework. Response surface models (RSMs) were developed to quantify the influence of geometric parameters and their interactions across loading conditions and evaluation positions. An analytical linear-elastic fracture mechanics (LEFM) model provided an independent computational reference for geometry-dependent fatigue strength. By transforming LEFM-derived nominal fatigue strengths using method-specific SCFs, the ability of each stress definition to account for geometric effects was assessed through correlation and residual scatter. Substantial differences between the approaches depended on joint geometry, loading condition, and evaluation position. Chord loading was mainly influenced by thickness ratio and brace slenderness, whereas brace loading additionally depended on

chord slenderness and diameter ratio. The XY method showed the strongest agreement with the LEFM-based reference and the lowest residual scatter, followed by Dong's method, whereas conventional surface-extrapolation approaches exhibited greater scatter. These findings highlight limitations of directly transferring established CHS-based extrapolation procedures to monopile attachments with pronounced geometric scale differences.

Keywords: Finite Element Analysis, Structural Stress, Circular Hollow Sections, Fatigue, Design of Experiments, Linear Elastic Fracture Mechanics

1 Introduction

Offshore wind turbine support structures are subjected to highly variable cyclic loads induced by wind and wave loading [1]. For monopile foundations, these actions result in global axial forces and bending moments in the primary support structure and lead to fatigue-relevant stress ranges [2]. Secondary steel attachments, such as boat landings, may introduce additional fatigue-critical locations because geometric discontinuities and local stiffness changes disturb the stress field of the monopile shell [3]. Boat landing structures are commonly connected to the monopile or transition piece by welded tubular hollow section and are exposed to cyclic environmental and operational loads, see Figure 1. Wave-induced loads acting on the boat landing generate bending moments in the attached braces, whereas axial brace forces may result from boat impact, wave loading and load redistribution within the secondary frame. Numerical investigations of impact-loaded offshore steel substructures further demonstrate that vessel-impact loads acting on secondary components are transferred into the primary structure, resulting in local stress concentrations [4]. In addition, the boat landing may locally restrain the bending deformation of the monopile shell. The resulting deformation compatibility between the primary shell and the secondary boat landing frame induces constraint forces and secondary bending stresses in the joint region. Consequently, the stress state at the welded connection is governed by the interaction of global monopile loading, local brace loading and attachment-induced stiffness changes.

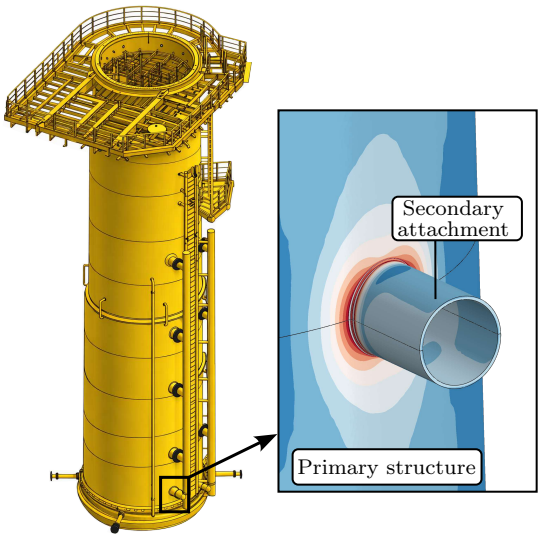


Fig. 1 Welded secondary attachment on transition piece shell (source: IPU Ingenieurgesellschaft Braunschweig mbH, Braunschweig, Germany)

Stress concentration factors (SCFs) in welded tubular joints have been investigated extensively for different joint configurations, loading conditions and geometrical parameter ranges. Comprehensive reviews by Saini et al. [5] and Zavvar et al. [6] summarize experimental and numerical investigations on tubular joints, covering SCFs, structural stresses, fatigue behavior and related design provisions. These reviews highlight the strong dependency of the local stress response on joint geometry, loading mode and evaluation position, while also identifying remaining limitations of existing design approaches. Atteya et al. [7] combined experimental measurements and finite-element analyses (FEA) to investigate elastic SCFs in tubular joints, demonstrating the strong dependency of the local stress field on the joint geometry. More recently, Yang et al. [8] investigated large-scale welded tubular T-joints experimentally and numerically, providing particular relevance to tubular connections with dimensions beyond conventional laboratory-scale specimens. In addition to deterministic SCF investigations, probabilistic and data-driven approaches have increasingly been employed to describe geometrical influences. The strong dependency of dimensionless joint parameters on the SCFs has also been demonstrated by Zavvar et al. [9], who identified pronounced effects of the wall-thickness ratio τ, diameter ratio β and chord slenderness γ_0, with the governing influence additionally depending on the evaluated weld-toe position. Liang et al. [10] developed probabilistic SCF models for concrete-filled tubular joints under axial loading and in-plane bending, whereas Iqbal et al. [11] applied finite-element-based artificial neural networks to predict SCFs in tubular KT-joints under combined loading. For the joint configuration considered in the present study, a previous study applied a Design of Experiments and Response Surface Model (DoE–RSM) framework to identify the governing geometrical parameters for chord-side HSS under axial brace loading [12]. However, these investigations remain

focused on geometrical SCF prediction and do not address the suitability of different structural stress definitions for fatigue assessment. These studies demonstrate the increasing capability to represent complex parameter dependencies but remain primarily focused on the prediction of SCFs for specific tubular-joint configurations.

A separate aspect concerns the definition of the fatigue-relevant structural stress itself. Vieira Ávila et al. [13] systematically compared IIW [14, 15] and DNV [16] hot-spot stress (HSS) evaluation procedures for welded tubular KT-joints and demonstrated that the selected numerical procedure can lead to relevant differences in the resulting SCFs. Recent investigations by Machač et al. [17] further indicate that the interpretation of HSS and thickness effects remains sensitive to the considered hollow-section geometry and wall-thickness range. These observations are particularly relevant for monopile secondary attachments, whose geometry may deviate substantially from the configurations underlying established tubular-joint recommendations. The investigated detail differs from conventional tubular joints by the pronounced scale difference between the monopile shell and the attached brace and the brace orientation. Moreover, the comparatively small brace-to-chord diameter ratio β and large chord slenderness γ_0 place substantial parts of the investigated parameter space outside the applicability ranges underlying conventional CHS-based formulations [16, 18, 19], as illustrated in Figure 2 and Figure 4. The direct transfer of established CHS-based surface-extrapolation procedures to such joints is therefore uncertain. Alternative structural stress approaches, such as the Xiao–Yamada (XY) 1 mm stress method [20] and the structural stress method proposed by Dong [21], provide fundamentally different representations of the fatigue-relevant stress field and are therefore considered alongside the conventional extrapolation approaches. A systematic comparison is therefore required to determine how consistently these approaches represent the geometry-dependent fatigue response under different loading conditions and at different evaluation positions.

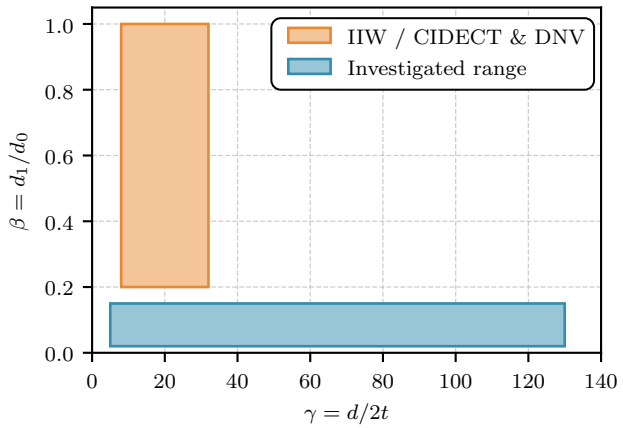


Fig. 2 Comparison of the investigated parameter range with the applicability ranges of conventional tubular-joint SCF formulations [16, 18, 19]

Against this background, the present study addresses three main questions:

1. How do established structural stress approaches quantitatively differ when applied to single-sided welded CHS joints with pronounced geometric scale differences?
2. How consistently do the individual stress definitions account for the geometry-dependent fatigue response predicted by an independent LEFM-based reference?
3. Which geometrical parameters govern the chord-side stress concentration, and how do these dependencies vary with loading condition and evaluation position?

To address these questions, five structural stress approaches are evaluated within a common linear-elastic FE framework. Their geometry-dependent response is investigated using a DoE–RSM approach, while analytical linear-elastic fracture mechanics (LEFM) provides a stress-definition-independent computational reference for assessing the consistency of the resulting SCFs. This combined framework enables both the comparison of the structural stress definitions and the identification of the governing geometrical effects.

2 Methodology

The general methodological framework of the study is illustrated in Figure 3 and comprises two coupled analysis branches. In the FE-based branch, the relevant geometrical parameters were first investigated by a screening DoE, followed by a main DoE and the derivation of RSMs for the different loading conditions, evaluation paths, and structural stress approaches. The resulting SCFs extracted from the RSM were subsequently compared against the underlying FE results and used to analyze the geometry-dependent stress response. In a second branch, analytical LEFM was employed to derive a fatigue reference independent of the investigated structural stress definitions. Finally, both branches were combined by relating the method-specific SCFs to the LEFM-derived fatigue strengths in order to assess how consistently the individual stress approaches represent the geometry-dependent fatigue response. The individual components of the framework are described in the following sections.

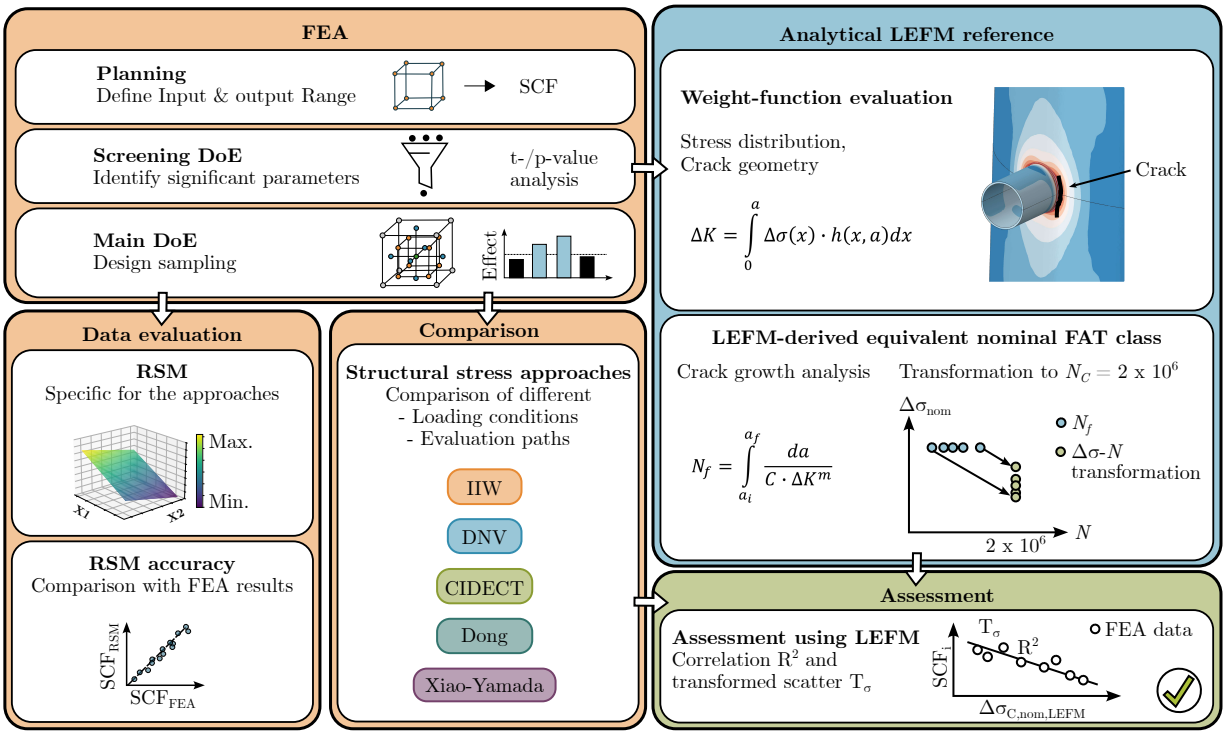


Fig. 3 Flowchart using DoE-RSM [22, 23] and analytical LEFM [24] for evaluating different structural stress fatigue approaches

2.1 System and range of variables

Figure 4 illustrates the design of the investigated tubular joint, which consists of two welded CHS. The figure also defines the dimensionless parameters used to describe the joint geometry and to parametrize the subsequent numerical study.

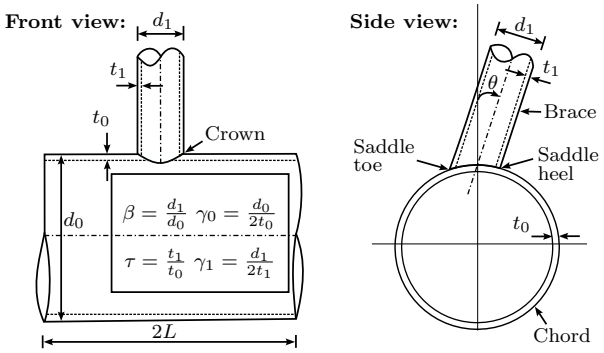


Fig. 4 Definition of dimensionless and dimensional parameters

Table 1 summarizes the dimensionless and dimensional parameters considered in the numerical parameter study. A wide parameter range was investigated in order to systematically evaluate the resulting SCFs for different tubular joint configurations and loading conditions. Although parts of the selected parameter range extend beyond typical boat-landing geometries, this range was intentionally included to investigate the general applicability and limitations of the considered structural stress approaches for tubular joints with pronounced scale differences. The normalized chord length was defined as $\alpha = \frac{2L}{d_0}$ and was kept constant at $\alpha = 2$ throughout the present study. Consequently, the derived results are conditional on the selected chord length and boundary configuration. The stress evaluation was focused on the chord surface, since the fatigue assessment in this study targets the stress concentration in the primary structure.

Table 1 Parameter ranges used in the DoE

Type	Parameter	Range	Unit
Dimensionless	β	$[0.015 - 0.15]$	–
	γ_0	$[28 - 130]$	–
	γ_1	$[5 - 30]$	–
	τ	$[0.05 - 0.5]$	–
Dimensional	θ	$[0 - 25]$	°
	d_1	$[165 - 2270]$	mm
	d_0	$[2000 - 12500]$	mm
	t_1	$[2.5 - 55]$	mm
	t_0	$[50 - 200]$	mm

2.2 Structural stress fatigue approaches

2.2.1 Surface extrapolation for plate structures

The IIW surface extrapolation approach for plate-type welded joints determines the HSS from surface stresses evaluated at defined distances in front of the weld toe [14, 15].

The method is based on the separation between the HSS σ_{HS} caused by the global joint geometry (membrane stresses σ_M and bending stresses σ_b) and the local nonlinear notch stress σ_{nl} caused by the weld profile. The stress increasing part of the weld profile should not be included in the extrapolated HSS, but is implicitly accounted for by the corresponding fatigue resistance curve. For type-a hot spots, where the weld toe is located on the plate surface, the structural surface stress component perpendicular to the weld toe is evaluated along a path normal to the weld toe [14]. A relatively fine finite-element mesh is required when high stress gradients occur close to the weld toe, as expected for complex welded details and local attachment geometries [14]. In such cases, the refined discretization enables a reliable evaluation of the structural stress field at the prescribed extrapolation points, while avoiding the notch-dominated and potentially singular stress field directly at the weld transition [14]. For a fine mesh condition, the IIW recommendation defines a linear extrapolation using the stresses at distances of $0.4 \times T$ and $1.0 \times T$ from the weld toe, where T denotes the wall thickness of the evaluated component, see Figure 5. The element size normal to the weld toe should be $\leq 0.4 \times T$ [15]. This allows the structural surface stress gradient to be resolved up to the first reference point and avoids evaluating the HSS from a discretization that is too coarse for the prescribed extrapolation distances.

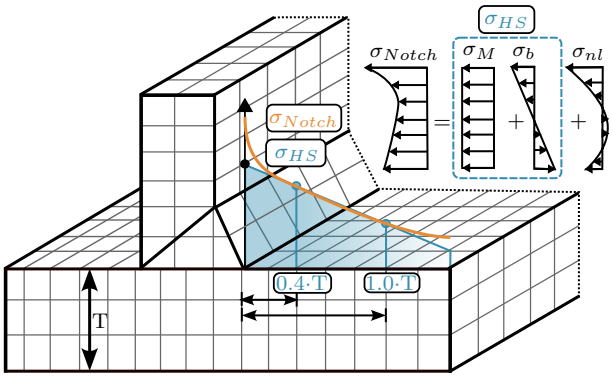


Fig. 5 IIW Plate structures surface extrapolation [14]

2.2.2 Surface extrapolation for CHS

For welded CHS joints, the HSS is also determined by surface stress extrapolation. The basic procedure is identical to the IIW approach for plate structures [14]: surface stresses are evaluated along an evaluation path normal to the weld toe at two defined reference points and are linearly extrapolated to the weld toe. The local nonlinear weld notch stress directly at the weld toe is therefore excluded from the evaluation, while the structural stress concentration caused by the joint geometry and load transfer is retained. The difference between the CHS-based recommendations therefore does not lie in the extrapolation principle itself, but in the definition of the reference point locations. The IIW/CIDECT recommendation [18, 19] defines the first reference point in the same area as the IIW recommendation for plate structures [14], at a distance of $0.4 \times T$ from the weld toe. The second reference point is defined as a function of

the tubular joint geometry. Depending on the evaluated position, i.e. crown or saddle, the second reference distance accounts for the radii and wall thicknesses of the brace and chord. Thus, the IIW/CIDECT formulation introduces the influence of the CHS geometry primarily through the second extrapolation point, see Table 2. CIDECT specifies a local finite-element mesh size of approximately $0.5 \times T$ to $0.5 \times t$ for numerical SCF determination, while requiring a mesh-sensitivity study to demonstrate that further mesh refinement does not significantly affect the computed stress distribution or resulting SCFs.

Table 2 Reference points for HSS calculation according to IIW/CIDECT [18, 19] and DNV [16]

Code	**Reference-point**	**Chord crown**	**Chord saddle**
IIW [18] / CIDECT [19]	a	$0.4T$	$0.4T$
	b	$0.4\sqrt[4]{rtRT}$	$0.09R$
DNV-RP-C203 [16]	a	$0.2\sqrt{rt}$	$0.2\sqrt{rt}$
	b	$0.4\sqrt[4]{rtRT}$	$\pi R/36$

In contrast, DNV-RP-C203 [16] defines both reference points as geometry-dependent distances. Depending on the evaluated position, the reference-point distances depend on the member radii and/or wall thicknesses. Accordingly, the DNV approach accounts for the curvature and thickness of the CHS joint already at the first extrapolation point. DNV-RP-C203 additionally allows a direct evaluation of the HSS at Gaussian integration points, if these are positioned $0.1 \times \sqrt{rt}$ from the weld toe, with r and t denoting the radius and wall thickness of the considered tubular member. In this case, the stress at the Gaussian point may be used directly for fatigue assessment instead of applying a two-point extrapolation. These procedures may lead to reference point locations that differ considerably from the plate structure IIW extrapolation [14], particularly for large diameter and thick-walled monopile connections. The location of the reference points for CHS is illustrated schematically in Figure 6.

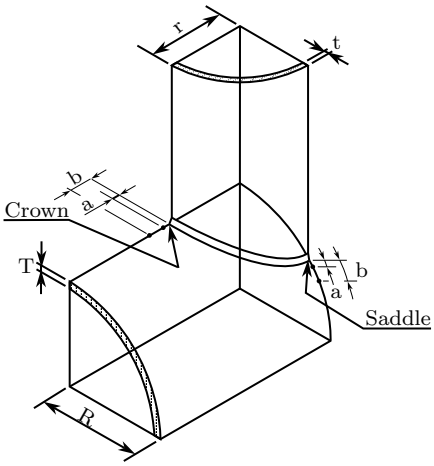


Fig. 6 Extrapolation reference points according to IIW/CIDECT [18, 19] and DNV [16]

2.2.3 XY structural stress

The XY method [20] is an alternative structural stress approach for welded joints in which the fatigue-relevant geometric stress is not obtained by surface extrapolation, but by evaluating the stress 1 mm below the weld toe surface in the expected crack propagation direction, see Figure 7. A central assumption of the method is that the evaluated stress is located outside the highly mesh-sensitive, non-linear weld notch stress field, but still sufficiently close to the weld toe to capture the structural stress concentration governing early crack propagation. Xiao and Yamada show that the weld toe stress itself is strongly affected by the local weld toe radius, toe angle and finite-element mesh size, whereas the stress approximately 1 mm below the surface is considerably less sensitive to these parameters. For large-scale structural models, the direct use of element sizes below 1 mm in the entire model is generally computationally inefficient, therefore, a submodel strategy should be adopted, in which the global model provides the boundary conditions for a locally refined submodel of the weld toe region.

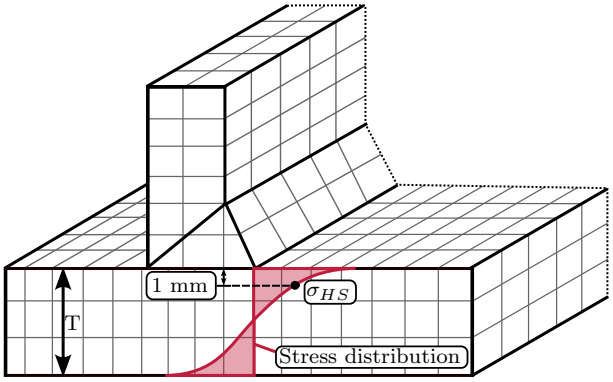


Fig. 7 XY 1 mm stress evaluation [20]

In contrast to conventional surface-extrapolated HSS, the 1 mm stress also accounts for size and plate-thickness effects through the stress gradient along the prospective crack path. Consequently, when fatigue assessment is consistently based on the XY 1 mm stress and the corresponding fatigue resistance, no additional thickness correction of the fatigue class is required. Thus, structural stress according to the XY approach is defined as the normal stress evaluated 1 mm below the weld toe surface along the expected crack propagation path:

$$\sigma_{HS} = \sigma_{(s=1\,\mathrm{mm}),} \tag{1}$$

where s denotes the distance from the weld toe along the expected crack path.

2.2.4 Dong structural stress method

The structural stress methods proposed by Dong [21, 25] – as they are in principle included by the American Society of Mechanical Engineers (ASME) in the Boiler and Pressure Vessel Code [26] of the Fitness for Service Code [27] – define the fatigue-relevant structural stress at the weld toe based on membrane and bending stress components evaluated at the fatigue critical cross section. The structural stress is expressed as

$$\sigma_s = \sigma_m + \sigma_b, \tag{2}$$

where σ_m and σ_b denote the membrane and bending components, respectively. This approach is based on a force and moment equilibrium across a critical cross section through the weld toe. There are two evaluation routes:

1. force and moment based approach: Nodal forces (in solid models) or nodal forces and moments (in shell models) are used. The resulting structural stresses are mesh-insensitive
2. stress based approach: The stress determined on a path through a critical cross section of a component is used. Only stresses normal to the path respectively normal to the weld are evaluated. The resulting structural stresses show a mesh-sensitivity.

The latter one is used in this paper and, therefore, described in more detail.

The evaluation uses the same stress path as it is used for the evaluation according to XY approach and the fracture mechanical evaluation. In a first step, the membrane stress is evaluated

$$\sigma_m = \frac{1}{t}\int_0^t \sigma(y)dy. \tag{3}$$

Then, the bending part is derived

$$\sigma_b = \frac{6}{t^2}\int_0^t \sigma(y)\left(\frac{t}{2} - y\right)dy. \tag{4}$$

Finally, the structural stress is determined by Equation 2.

2.3 Independent fatigue reference based on analytical LEFM

In addition to the evaluation with structural stresses, a fracture mechanical evaluation is conducted. The stresses perpendicular to the path through the critical cross section that starts at the weld toe are used and are multiplied by a factor of 200 to achieve a cyclic stress intensity factor $\Delta K > \Delta K_{th} = 2\,\mathrm{MPa}\sqrt{\mathrm{m}}$. Stress intensity factors as a function of the crack depth $K = f(a)$ are evaluated by weight functions according to Shen et al. [24]:

$$\Delta K = \int_0^a \Delta\sigma(x)\; h(x,a)\,\mathrm{d}x, \tag{5}$$

where x denotes the distance from the weld toe along the prospective crack path and $h(x,a)$ is the geometry-dependent weight function. An initial crack with a depth of $a_i = 0.1\,\mathrm{mm}$ and a width of $c = a$ is used as recommended by IIW [15]. The propagation of the crack was calculated using the Paris law [28]:

$$\frac{\mathrm{d}a}{\mathrm{d}N} = C\,(\Delta K)^{m_p}\,. \tag{6}$$

Material values are also adopted from IIW [15] with $C = 1.8 \times 10^{-13}$ and $m_p = 3$. The calculation is stopped as the crack reaches half the chord wall thickness. The results are the number of cycles to failure N_f. To enable a comparison with results from the structural stress approach, the number of cycles are transformed to stresses

$$\Delta\sigma_{C,nom,LEFM} = 200\,\mathrm{MPa} \times \left(\frac{N_f}{2 \times 10^6}\right)^{1/3}. \tag{7}$$

A derivation of stress concentration factors, as they result from all structural stress approaches, is not possible. The resulting $\Delta\sigma_{C,nom,LEFM}$ is referred to as the LEFM-derived equivalent nominal FAT class. It represents the nominal stress range corresponding to the calculated LEFM fatigue life when transformed to the reference load cycles $N_C = 2 \times 10^6$ using the adopted S–N slope $m = 3$. The quantity is used as a computational reference and does not represent an experimentally calibrated FAT class.

2.4 Assessment procedure for structural stress approaches

The LEFM-derived nominal fatigue strength $\Delta\sigma_{C,LEFM}$ was subsequently used as a reference for evaluating the investigated structural stress approaches. Two complementary measures were considered. First, the relationship between the method-specific SCFs and the corresponding LEFM-derived nominal fatigue strengths was quantified by linear regression in log–log space. For this purpose, both quantities were transformed using the base-10 logarithm according to

$$log_{10}(SCF_{j,i}) = a + b \cdot log_{10}(\Delta\sigma_{C,j,nom,LEFM}), \tag{8}$$

where a and b denote the regression coefficients. The coefficient of determination R^2 was calculated from the logarithmically transformed values and was used to quantify

how consistently the geometry-dependent trend in fatigue strength is reflected by the corresponding SCFs. Second, the LEFM-derived nominal fatigue strength was transformed to the structural-stress level of each investigated approach. Under linear-elastic conditions, the structural stress range is related to the nominal stress range through the corresponding SCF. Accordingly, for geometry j and stress approach i, the transformed fatigue strength was calculated as

$$\Delta\sigma_{C,HS,j,i} = SCF_{j,i} \times \Delta\sigma_{C,j,nom,LEFM}. \tag{9}$$

If the respective SCF fully accounts for the geometry-dependent stress concentration governing the LEFM-based fatigue response, the transformed fatigue strengths should become largely independent of the investigated joint geometry. The remaining scatter T_σ therefore provides a measure of the consistency with which the respective stress definition normalizes the geometry-dependent LEFM fatigue resistance, quantified by

$$T_\sigma = \frac{Q_{90}(\Delta\sigma_{C,HS,i})}{Q_{10}(\Delta\sigma_{C,HS,i})}, \tag{10}$$

where Q_{90} and Q_{10} denote the 90th and 10th quantiles of the transformed fatigue-strength distribution, respectively. A lower T_σ therefore indicates a more consistent normalization of the geometry-dependent LEFM fatigue strength by the respective structural stress definition.

2.5 DoE and RSM

A conventional one-variable-at-a-time (OVAT) approach would require a large number of finite-element simulations, since all parameters except one are kept constant in each variation step. This limits the efficient identification of interaction effects between the governing parameters and becomes computationally inefficient for the considered multidimensional parameter space [22]. Therefore, a numerical Design of Experiments (DoE) framework was used. The general DoE–RSM procedure follows the methodology previously applied to the considered joint configuration, where the screening design, central composite inscribed (CCI) sampling strategy and statistical model evaluation are described in greater detail [12]. In the present study, this framework was extended to multiple loading conditions, evaluation paths and structural stress assessment approaches. By varying several parameters simultaneously according to a statistically defined design plan, the DoE approach reduces the required number of simulations while enabling the systematic evaluation of main effects, interaction products and nonlinear parameter influences on the resulting SCFs. The selected input parameters describe the relevant geometric and loading-related characteristics of the joint and were systematically varied within predefined limits. For each design point, a finite-element model was generated and evaluated, and the resulting SCFs were extracted. The focus of the present study is placed on the chord-side SCF, since the objective is to assess the fatigue-relevant stress concentration in the primary load-bearing structure. The brace-side SCF is therefore not considered as the governing evaluation parameter in the subsequent modeling. The DoE was divided into a screening stage and a subsequent main design stage. In the screening stage, a two-level full factorial design

was used to identify the relevant input parameters and interaction products for each loading condition and evaluation path [23]. The factors were evaluated at their lower and upper bounds, while replicated center points were included to estimate the error variance. A linear regression model comprising main effects and selected two-factor interactions was fitted to the screening data. The governing parameters were identified from Pareto diagrams of the standardized t-values, where effects exceeding the critical threshold corresponding to a significance level of 5% were classified as statistically significant. Non-significant factors were excluded from the final response surface formulation, while the governing parameters were retained for the main DoE evaluation. This reduced the complexity of the regression models and avoided overfitting terms that do not contribute significantly to the SCF prediction. The main experiments were then planned, using a CCI design, which enables the estimation of linear, interaction and quadratic effects within the predefined parameter limits. The resulting main design was used to derive the final response surfaces for the selected output quantities. For a CCI design with k input parameters, the number of required simulations N is given by

$$N = 2^k + 2k + n_c, \tag{11}$$

where 2^k denotes the factorial design points, $2k$ the axial points and n_c the number of center points. In the inscribed variant, the axial points are scaled such that all design points remain within the predefined parameter limits. For each combination of loading condition, evaluation path and HSS approach, an individual RSM was derived. The SCF was treated as the response variable, while the dimensionless geometrical parameters and, where applicable, the brace inclination were used as input variables. Linear, interaction and quadratic terms were considered during model development. The general second-order response surface, commonly used to represent linear, quadratic and interaction effects in RSM, can be written as [29, 30]

$$\hat{y} = \beta_0 + \sum_{i=1}^{k} \beta_i X_i + \sum_{i=1}^{k} \beta_{ii} X_i^2 + \sum_{i=1}^{k-1} \sum_{j=i+1}^{k} \beta_{ij} X_i X_j, \tag{12}$$

where $\hat{y}$ denotes the predicted response, β_0 the intercept, β_i,β_{ii} and β_{ij} the regression coefficients associated with linear, quadratic and interaction products. X_i and X_j are the independent input variables. The final reduced equations retained only statistically significant terms. The goodness of fit and predictive capability of the reduced RSMs were assessed using the coefficient of determination R^2 and the predicted coefficient of determination R^2_{pred}, respectively. The coefficients were calculated as

$$R^2 = 1 - \frac{\sum_{i=1}^{n} (y_i - \hat{y}_i)^2}{\sum_{i=1}^{n} (y_i - \bar{y})^2} \tag{13}$$

and

$$R^2_{\text{pred}} = 1 - \frac{\sum_{i=1}^{n} \left(y_i - \hat{y}_{(i)}\right)^2}{\sum_{i=1}^{n} \left(y_i - \bar{y}\right)^2}, \tag{14}$$

where y_i denotes the FE-derived SCF, $\hat{y}_i$ the corresponding RSM prediction, and $\bar{y}$ the arithmetic mean of the FE-derived SCFs. The predicted coefficient of determination was obtained by leave-one-out cross-validation. Accordingly, $\hat{y}_{(i)}$ denotes the prediction of observation i obtained from a regression model fitted to the remaining $n-1$ observations. In addition, the normalized root-mean-square-error (NRMSE) was used to quantify the magnitude of the deviation between the RSM approximation and the corresponding FE-derived SCFs. To allow comparison between data sets with different absolute SCF levels, the RMSE was normalized by the arithmetic mean of the FE-derived SCFs:

$$\text{NRMSE} = \frac{\sqrt{\frac{1}{n}\sum_{i=1}^{n} \left(SCF_{\text{RSM},i} - SCF_{\text{FEA},i}\right)^2}}{\overline{SCF}_{\text{FEA}}} \times 100\,\%. \tag{15}$$

Since different HSS approaches may lead to different fatigue-relevant stress parameters, the described DoE–RSM workflow was applied consistently to all investigated assessment approaches. In this way, the influence of the selected structural stress definition on the predicted chord-side SCF can be evaluated on a consistent numerical basis.

3 Numerical analysis

3.1 FE model and loading conditions

The FEA was carried out in Abaqus/Standard 2025 using eight-node hexahedron elements with linear shape functions (element type C3D8R), while the weld geometry was discretized using six-node wedge elements with linear shape functions (C3D6). The material was defined as linear elastic, characterized by Young's modulus E (210 GPa) and Poisson's ratio υ (0.3). The geometries were generated automatically using a script-based and fully parametrized modeling procedure implemented through the Abaqus Python interface, enabling consistent model generation for all design points within the numerical DoE. The loading conditions investigated in this study are summarized in Table 3.

For the considered configurations, axial loading as well as in-plane bending (IPB) and out-of-plane bending (OPB) were analyzed in order to represent the relevant fatigue loading situations of the welded tubular joint. Depending on the applied loading direction, different stress concentrations occur at the chord-side crown and saddle regions. Therefore, load-case-specific evaluation paths were defined for the extraction of the structural stresses and the corresponding chord-side SCFs, as indicated in Figure 8.

Table 3 Loading conditions and evaluation paths for analyzed systems

Loading-Nr.	Item	Loading condition	SCF evaluation path
1	Chord	Axial	Crown
2		IPB	Crown
3	Brace	Axial	Crown, Saddle heel, Saddle toe
4		OPB	Saddle heel, Saddle toe
5		IPB	Crown

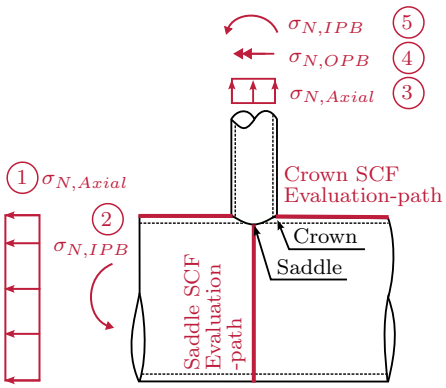


Fig. 8 Evaluation path of different loading conditions

3.2 Model reduction and boundary conditions

To reduce the computational effort of the FEA, geometric symmetry was exploited in the model generation. Since the investigated joint geometries are symmetric with respect to the X=0 plane, only one half of the structure was modeled, and a symmetry boundary condition was assigned to the cut surface, as illustrated in Figure 9. This reduced the number of elements and degrees of freedom while preserving the local stress field in the weld toe region.

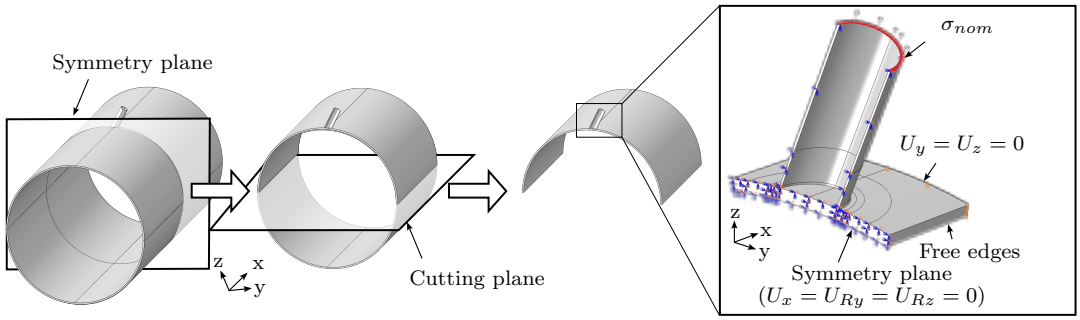


Fig. 9 Model reducing techniques

In addition, a model-reduction study was performed for the chord geometry. The results showed that the evaluated surface stresses are not sensitive when the circular chord circumference was reduced to a semicircular representation (cutting plane). Consequently, the chord geometry was also truncated in the x-y plane, leading to a further reduction of the model size without a relevant influence on the stress concentration at the chord-side evaluation paths (less than 1 %). A further distinction was required with respect to the load symmetry of the investigated load cases. Three boundary-condition systems were therefore defined, as shown in Figure 10.

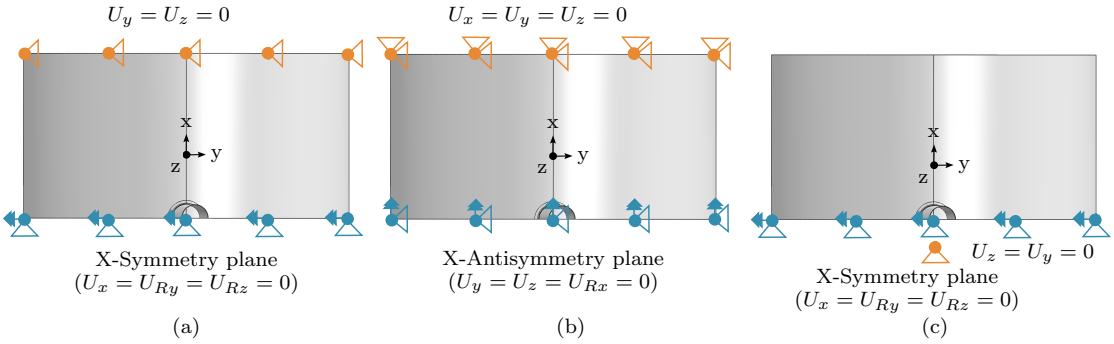


Fig. 10 Boundary conditions (a) Brace load axial & OPB (b) Brace load IPB (c) Chord Load Axial & IPB

System (a) was used for axial brace loading and brace OPB cases in which the deformation mode remains symmetric with respect to the vertical symmetry plane (Loading-Nr. 3,4). In this case, the cut surface was constrained by a symmetry boundary condition, while the brace load was applied to the reduced half model. System (b) was used for the IPB-bending load case, for which the geometry remains symmetric but the loading produces an antisymmetric deformation state with respect to the symmetry plane (Loading-Nr. 5). For this case, the symmetry boundary condition was replaced by an antisymmetric boundary condition in order to reproduce the deformation mode of the full model correctly. System (c) was used for loading of the

chord, including axial chord loading and chord bending (Loading-Nr. 1,2). In these load cases, the load was applied to the chord section of the reduced model. The same symmetry boundary condition at the vertical cut plane was retained, since the resulting deformation state is symmetric with respect to the model plane. In addition, a line boundary condition was introduced at the chord location where the circumferential tangent vector is horizontal. This boundary condition was used to transfer the reaction forces in the longitudinal direction of the chord and to suppress rigid-body motion without constraining the local deformation behavior in the weld-toe region.

3.3 Weld geometry idealization

In the present study, the weld geometry was idealized based on the American Welding Society (AWS) D1.1 [31] detailing concept for complete-joint-penetration tubular T-, Y- and K-connections. In this concept, the applicable weld detail is governed by the local dihedral angle ψ, which varies continuously along the brace–chord intersection, see Figure 11.

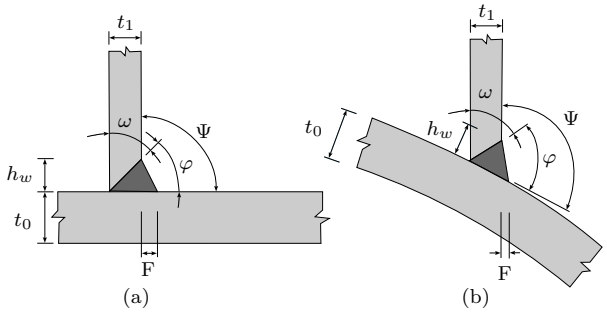


Fig. 11 Idealized weld profile based on AWS D1.1 [31], (a) Crown position, (b) Saddle position

Previous studies have shown that the local dihedral angle ψ directly affects the resulting SCF distribution [32]. Accordingly, the weld was generated from a sequence of local cross-sections along the intersection line, where ψ was determined from the tangent planes of the intersecting tubular members. For the numerical model, the chord-side toe-fillet size F was defined according to the standard flat profile concept shown in AWS D1.1 [31]. F varies linearly from zero at $\psi = 135°$ to $t_1/2$ at $\psi = 90°$. For smaller dihedral angles ψ down to $\psi = 50°$, F is kept constant at $t_1/2$. Thus, the toe-fillet size was described by the following piecewise function:

$$F = \begin{cases} 0, & 135° \leq \psi < 180°, \\ \dfrac{t_1}{2}\left[\dfrac{135° - \psi\,[°]}{45°}\right], & 90° \leq \psi < 135°, \\ \dfrac{t_1}{2}, & 50° \leq \psi < 90°. \end{cases} \tag{16}$$

where t_1 denotes the brace wall thickness. The parameter F therefore represents the idealized chord-side toe-fillet size used to construct the weld profile in the finite-element model. The resulting weld model represents an AWS-oriented idealized weld geometry and provides a consistent geometric basis for comparing the investigated structural stress concepts. Local as-built imperfections, such as weld toe irregularities, undercuts, convexity variations or deviations in weld shape, were not considered. While simplified approximations for the dihedral angle are available for standard T/Y-joint configurations with inclined braces, the specific joint geometries considered in this study required a manual determination of the relevant dihedral angles ψ in order to consistently define the weld cross-section around the intersection. From the generated cross-sections, continuous weld surfaces were constructed along the circumferential intersection line. These surfaces were subsequently closed to form watertight geometries and converted into solid weld volumes for finite element discretization. This procedure allowed the weld to be represented as an explicit solid part while maintaining a parametrized and reproducible model generation workflow.

3.4 SCF calculation

The SCF was calculated as the ratio between the HSS obtained from the structural stress concepts described previously and the corresponding nominal stress, as given in Equation (17). If the applied load is scaled such that the nominal stress equals a normalized stress of 1 MPa, the resulting SCF is numerically identical to the evaluated HSS. For all models, the fatigue-relevant stress was evaluated using the normal stress component acting perpendicular to the weld toe.

$$SCF = \frac{\sigma_{HS}}{\sigma_{nom}} \tag{17}$$

For the different loading situations, the normalized stresses were determined according to Equation (18) and Equation (19). In the axial load case, the normalized stress expression was rearranged with respect to the force N, whereas for in-plane and out-of-plane bending the bending stress expression was rearranged with respect to the bending moment M. Consequently, the applied force or moment was selected such that the nominal stress in the brace or chord cross-section was equal to 1 MPa, enabling a direct comparison of the resulting SCFs for all investigated geometries and loading conditions.

$$\sigma_{nom,\mathrm{Axial,Brace}} = \frac{4N}{\pi\left[d_1^2 - (d_1 - 2t_1)^2\right]} \tag{18}$$

$$\sigma_{nom,\mathrm{Bending,Brace}} = \frac{32 d_1 M}{\pi\left[d_1^4 - (d_1 - 2t_1)^4\right]} \tag{19}$$

3.5 Mesh discretization and sensitivity

3.5.1 Global model

The finite element mesh was divided into a locally refined region around the brace-chord intersection, a transition region and a coarse region, see Figure 12. The fine mesh

was used in the weld toe and hot-spot region to resolve the stress gradients governing the SCF evaluation, whereas the element size was gradually increased in the transition region to reduce the overall number of degrees of freedom. This strategy follows the general approach used in high-fidelity tubular-joint modeling, where a fine mesh is required near the weld, while coarser elements can be used away from the intersection because the stress gradients decrease with increasing distance from the weld.

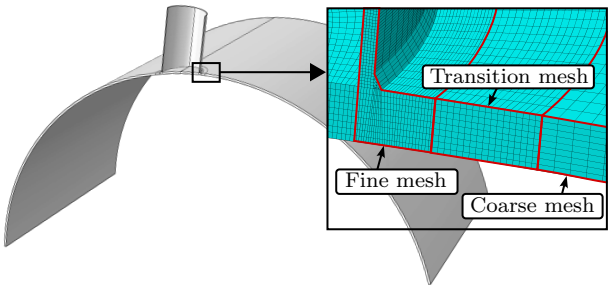


Fig. 12 Element mesh design

A mesh sensitivity study was carried out at the chord surface in the saddle region under axial brace loading, where high stress concentrations were expected. The objective was to identify a finite-element mesh that minimizes the computational effort while providing less mesh sensitivity stress results. As reference quantity, the SCF based on the IIW HSS approach for plate structures was used, since the corresponding reference points are located close to the weld toe and are therefore sensitive to the local mesh resolution. The mesh size was parametrized by the number of divisions through the chord wall thickness. Since the thickness ratio τ governs the relative brace-to-chord stiffness and was identified as a dominant parameter affecting the SCF, the mesh sensitivity study was performed for two limiting configurations corresponding to the minimum and maximum values of τ. These two cases represent the stiffness bounds of the investigated parameter range and were used to assess whether the selected discretization remains adequate for all intermediate configurations. The results of the mesh sensitivity study are shown in Figure 13. For comparison, the SCFs were normalized by the value obtained for the selected mesh with eight elements through the chord wall thickness, so that a normalized SCF of 1.0 corresponds to the selected discretization. From eight elements through the chord wall thickness onwards, further mesh refinement changed the resulting SCF by less than 3 %. This discretization was therefore applied consistently to all investigated FE models.

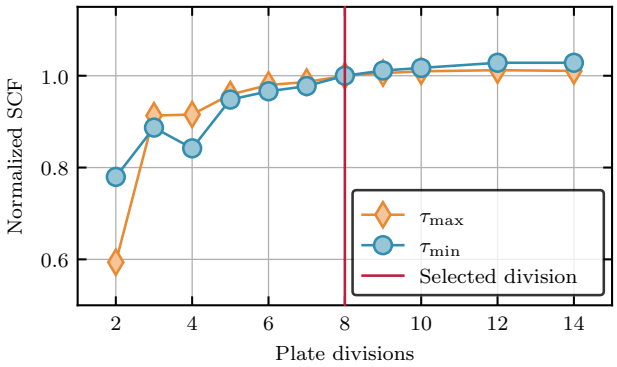


Fig. 13 Mesh sensitivity study for the chord-side saddle SCF under axial brace loading

3.5.2 Submodel for the XY approach

The XY approach requires the evaluation of the stress at a distance of 1 mm below the weld toe along the expected crack propagation path. Since the mesh resolution of the global FE models is not sufficient to resolve this local stress field accurately for the investigated wall-thickness range, a submodeling approach was employed. The submodel comprises the weld toe region and the surrounding parts of the brace and chord, while the displacement field obtained from the corresponding global model was transferred to the cut boundaries of the submodel. The extent of the submodel was selected such that the driven boundaries were sufficiently remote from the local weld-toe stress field and allowed the global deformation and load-transfer behavior to be represented without significantly constraining the local response. For this purpose, a radial distance of $3 \times t_0$, with t_0 denoting the chord wall thickness, was used between the weld-toe region and the outer cut boundary of the submodel. A separate mesh sensitivity study was performed for the locally refined weld-toe region using the XY stress evaluated 1 mm below the weld toe. As shown in Figure 14, the evaluated stress decreases with increasing mesh refinement and approaches an approximately constant value for sufficiently small element sizes. An element size of 0.25 mm was therefore selected for the local evaluation region, since further refinement resulted in only minor changes in the XY stress. This discretization provides four elements within the first 1 mm below the weld toe and was applied consistently to all XY submodels.

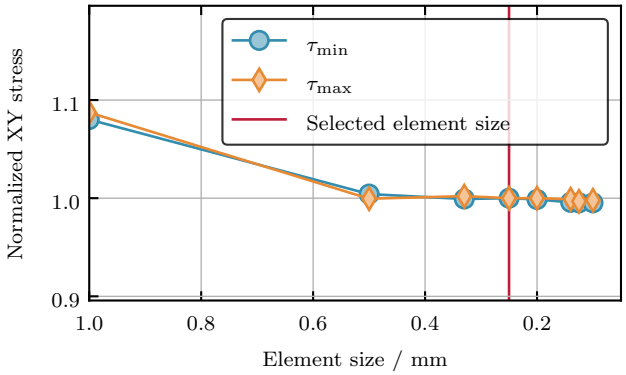


Fig. 14 Mesh sensitivity of the XY stress evaluated 1 mm below the weld toe

4 Results

4.1 Comparison of structural stress approaches

The comparison of the structural stress approaches was performed for each design point, loading condition, and evaluation path. For this purpose, the SCFs obtained directly from the FEA at the sampled DoE design points were used rather than the corresponding RSM predictions. Thus, the comparison is not affected by additional approximation errors introduced by the RSM. The IIW plate-structure approach was selected as reference for the relative comparison. This choice does not imply that the IIW plate approach represents an exact solution, but provides a consistent baseline independent of CHS-specific reference-point definitions. Figure 15 shows the resulting ratios between the method-specific SCFs and the corresponding IIW plate-structure SCFs. The DNV-based approach generally results in higher mean SCFs than the IIW plate extrapolation for all investigated loading conditions and evaluation paths. The positive deviations are more pronounced for several crown configurations, whereas the mean deviations at the saddle heel and saddle toe remain comparatively small but are likewise positive. The variation over the investigated parameter range indicates that the magnitude of the difference between the DNV and IIW plate approaches depends on both the joint geometry and the evaluated position. The IIW/CIDECT approach shows the closest agreement with the IIW plate extrapolation. At the crown positions, the mean SCF ratios remain close to unity, whereas slightly lower mean SCFs are obtained at the saddle heel and saddle toe. The comparatively small deviations are consistent with the similarity of the underlying surface-extrapolation procedures, although the geometry-dependent definition of the CHS reference points results in position-dependent differences. The XY approach yields systematically higher SCFs for the investigated brace-loading cases and exhibits the largest method-dependent deviations as well as the widest ranges over the considered parameter field. The most pronounced increase is observed for brace IPB at the crown position. For chord axial loading, by contrast, the deviation from the IIW plate reference is considerably smaller. The Dong approach generally results in moderate increases in SCF for brace loading,

with the largest deviation likewise occurring for brace IPB at the crown, whereas only minor differences are observed for chord axial loading.

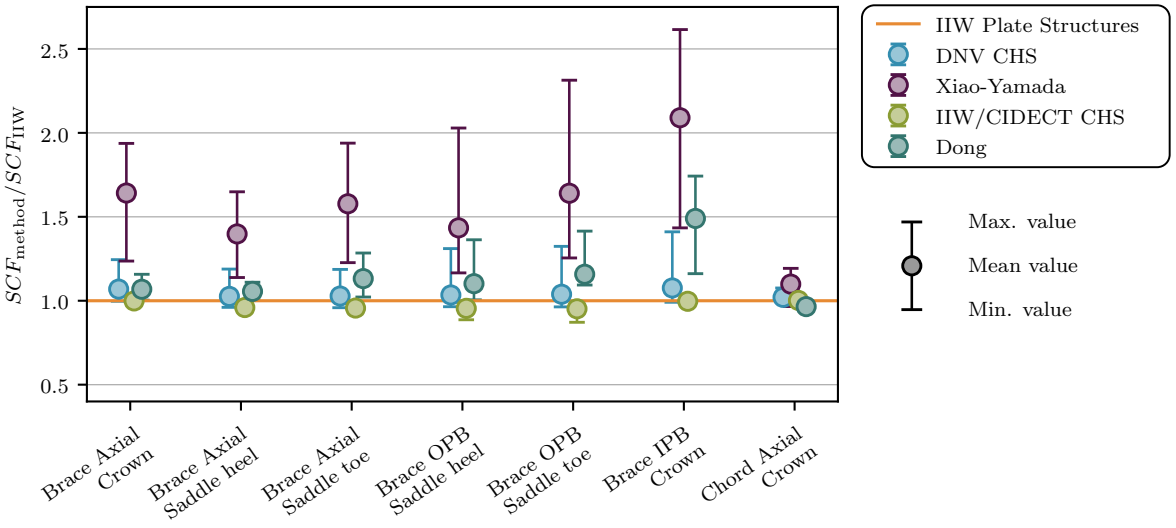


Fig. 15 Comparison of different structural stress approaches for different loading conditions and evaluation paths

Overall, the comparison demonstrates that the differences between the investigated structural stress approaches cannot be represented by a constant method-specific factor. Instead, their magnitude depends on the loading condition, evaluation position, and joint geometry. Particularly pronounced differences are obtained for the XY approach under brace loading, whereas the conventional surface-extrapolation procedures generally remain closer to the IIW plate reference. The mechanical origin of the observed method-dependent trends is discussed in Section 5 with particular consideration of the respective stress definitions and, for the surface-extrapolation approaches, the location of the prescribed reference points relative to the local stress gradient.

4.2 LEFM-based assessment of the structural stress approaches

For each investigated geometry and loading condition, the analytical LEFM model provides a calculated fatigue life based on the corresponding nominal stress range. To establish a common reference level, the calculated fatigue lives were converted into an equivalent nominal fatigue strength $\Delta\sigma_{C,LEFM}$ at $N = 2 \times 10^6$ cycles. The resulting LEFM-derived nominal FAT class inherently reflects the geometry-dependent influence on crack propagation contained in the LEFM solution. It is therefore used as an independent LEFM-based reference for evaluating the SCFs obtained from the different structural stress approaches. The LEFM-derived fatigue strength is not interpreted as an experimentally calibrated FAT class, but as a consistently calculated reference quantity for the investigated parameter field.

If a structural stress approach consistently represents the fatigue-relevant geometrical stress concentration, geometries associated with a low nominal LEFM fatigue strength are expected to exhibit correspondingly high SCFs, and vice versa. Figure 16 therefore compares the method-specific SCFs with the nominal FAT classes derived from LEFM. A pronounced correlation is observed for all investigated approaches, although the strength of the relationship differs between the methods. Thus, the XY and Dong approaches show the strongest relationship between the calculated stress concentration and the geometry-dependent fatigue resistance predicted by LEFM.

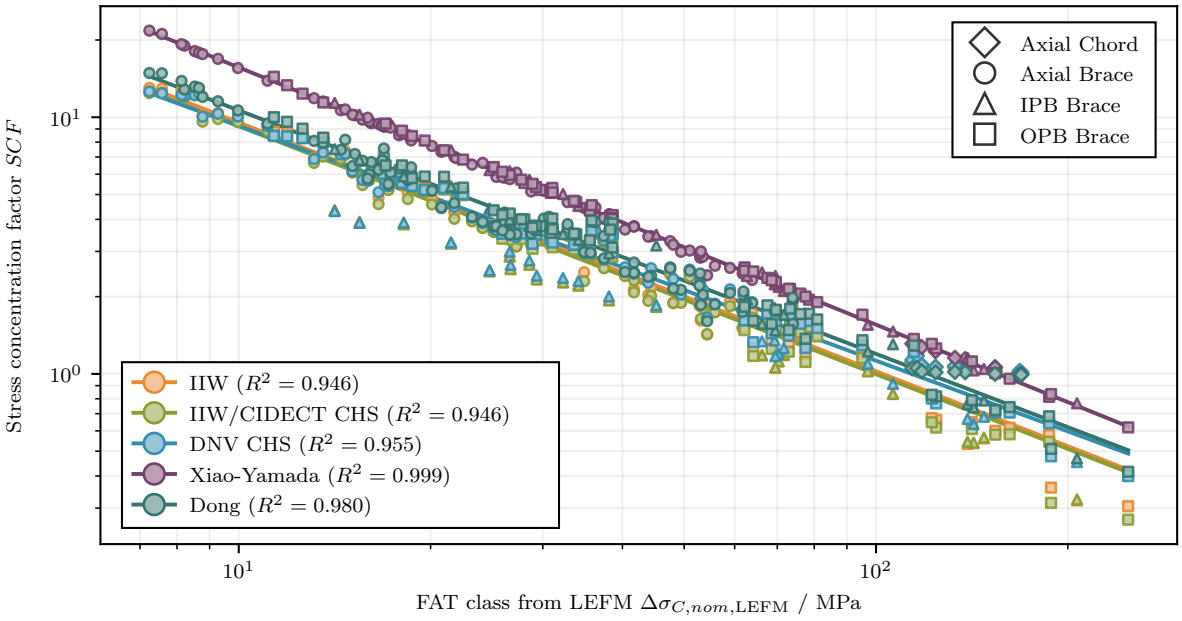


Fig. 16 Correlation between SCFs and FAT classes derived from LEFM

The transformed results to the structural stress level indicate that the XY stress definitions provide the most consistent transformation of the geometry-dependent nominal FAT class to a common structural stress level within the investigated parameter range, see Figure 17. The comparison therefore evaluates not only the magnitude of the calculated SCFs, but their ability to account for the geometrical effects that govern the LEFM-based FAT class.

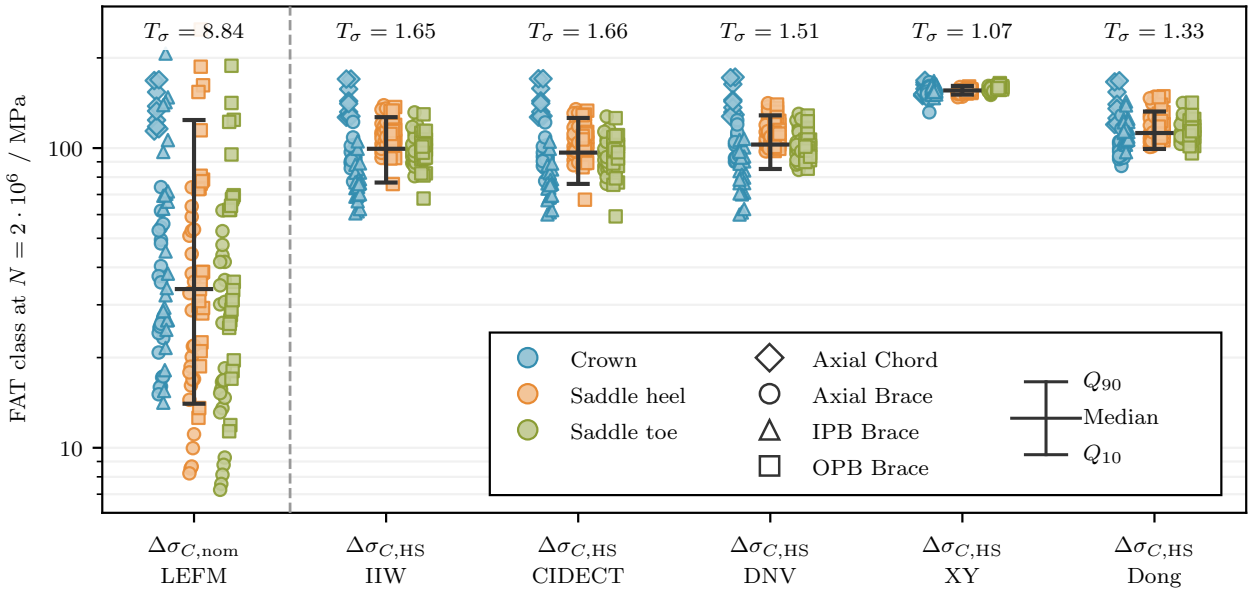


Fig. 17 Scatter of LEFM-derived fatigue strengths before and after transformation to the structural-stress level

4.3 Assessment of RSM Accuracy

Before using the RSMs to analyze the geometrical parameter effects in Section 4.4, their ability to reproduce the underlying FE results was assessed. The assessment of the derived RSM was evaluated by comparing the RSM-predicted SCFs with the corresponding FE-derived values. The assessment was performed individually for each loading condition and evaluation path. The assessment of the reduced RSMs was evaluated using the model-quality measures defined in Section 2.5. Table 4 summarizes the resulting model-quality measures for the investigated loading conditions and evaluation paths. The reported values represent the arithmetic mean across the five structural stress approaches. Overall, the RSMs show high coefficients of determination and comparatively small normalized deviations within the investigated parameter domain. The largest deviations occur for axial brace loading at the crown position, whereas the saddle-position models generally show higher coefficients of determination. The RSMs are therefore used in Section 4.4 as surrogate models for trend analysis within the investigated parameter domain, rather than as generally applicable SCF prediction equations.

Figure 18 compares the RSM predictions with the corresponding FE-derived SCFs for all investigated structural stress approaches, loading conditions and evaluation paths. The 10% and 20% lines are included as visual reference ranges. The inset provides an enlarged representation of the low-SCF range, for which relative deviations may appear comparatively large despite small absolute differences.

Table 4 Mean accuracy measures of the RSMs

Group of Loading-Nr.	Evaluation path	R^2_{mean}	$R^2_{\text{pred,mean}}$	$NRMSE_{\text{mean}}$ / %
1,2	Crown	0.96	0.91	1.30
3	Crown	0.95	0.88	9.22
3	Saddle heel	0.99	0.96	6.12
3	Saddle toe	0.99	0.97	5.69
4	Saddle heel	0.99	0.98	6.18
4	Saddle toe	0.99	0.98	6.27
5	Crown	0.99	0.97	5.23

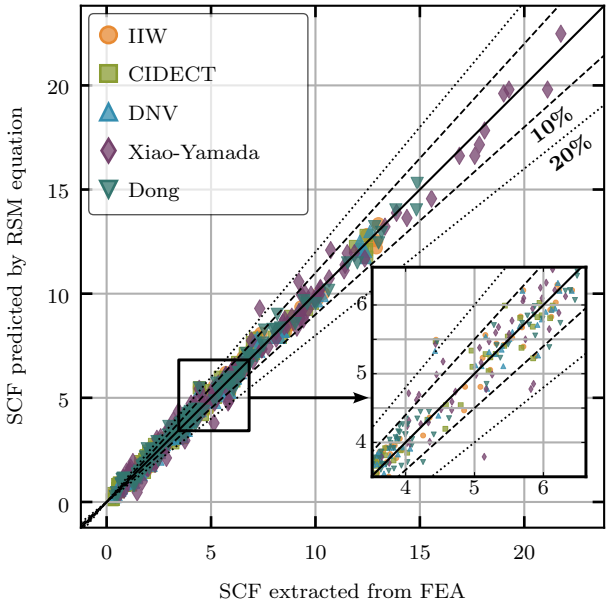


Fig. 18 Comparison of RSM-predicted and FE-derived SCFs for all investigated loading conditions, evaluation paths and structural stress approaches.

4.4 Geometrical effects on the SCF

4.4.1 Screening and retained parameters

The geometrical parameters exhibiting a statistically significant influence on the SCF are summarized in Table 5. The screening analysis considered the dimensionless parameters β, γ_0, γ_1, and τ, together with the brace inclination θ. A parameter was classified as influential when its effect was statistically significant at a significance level of $p < 0.05$. The identified parameter dependencies differ between chord and brace loading. For chord loading, only the thickness ratio τ and brace slenderness γ_1 showed a significant influence. For brace loading, the SCF was consistently influenced by τ,

γ_0, and β, while an additional influence of the brace inclination θ was identified for selected loading conditions and evaluation paths.

Table 5 Screening results of significant effects on the SCF

Group of Loading-Nr.	Evaluation path	Significant parameters
1,2	Crown	τ, γ_1
3	Crown	$\tau, \gamma_0, \beta, \theta$
3	Saddle heel	$\tau, \gamma_0, \beta, \theta$
3	Saddle toe	τ, γ_0, β
4	Saddle heel	τ, γ_0, β
4	Saddle toe	τ, γ_0, β
5	Crown	$\tau, \gamma_0, \beta, \theta$

The screening analysis reduced the initial five-parameter description to a maximum of four relevant parameters for the individual loading conditions and evaluation paths. The governing parameters were found to depend distinctly on the applied loading mode. For brace loading, the SCF is primarily controlled by the diameter ratio β, the chord slenderness γ_0 and the thickness ratio τ, while the brace inclination θ contributes only for selected evaluation paths. The identified significant parameters were subsequently retained as input variables for the main DoE and systematically evaluated with respect to their linear effects, two-factor interactions, and quadratic effects on the SCF.

4.4.2 Chord loading (Axial and bending)

For chord loading, the relevant chord-side stress concentration occurs at the crown position, consequently, only the crown evaluation path was considered for axial loading and in-plane bending of the chord. Both loading conditions showed the same significant geometrical parameters and qualitatively similar response-surface characteristics and are therefore discussed jointly. The screening analysis identified the thickness ratio τ and the brace slenderness γ_1 as significant parameters. In the subsequent main DoE, the interaction term $\tau\gamma_1$ and the quadratic term τ^2 were additionally retained in the reduced RSM. Figure 19 shows the resulting response surface for the IIW approach as a representative example. The investigated structural stress approaches exhibited qualitatively similar parameter dependencies despite differences in the absolute SCF level and regression coefficients. The SCF is primarily affected by τ, while the influence of γ_1 is less pronounced. The retained interaction term indicates that the effect of τ depends on the brace slenderness, whereas the quadratic term reflects a nonlinear dependence on the thickness ratio. Within the investigated parameter range, increasing γ_1 generally reduces the SCF.

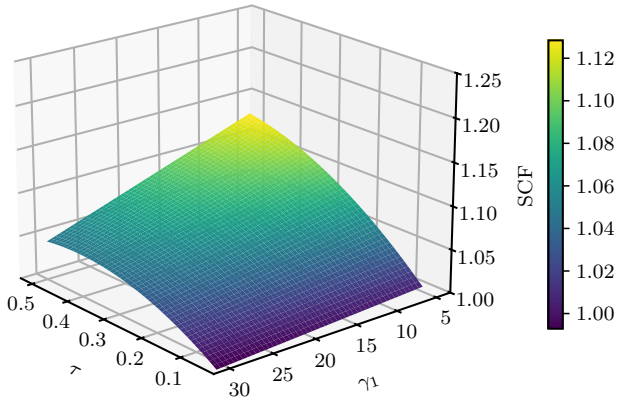


Fig. 19 Axial and IPB chord loading, IIW plate approach, Crown position

The influence of τ can be associated with the relative wall-thickness configuration and thus with the stiffness ratio between the brace and the chord shell, whereas γ_1 characterizes the slenderness and local stiffness contribution of the attached brace. The retained RSM terms for chord loading are summarized in Equation (20).

$$SCF_{\text{Axial/Bending Chord loading}} = f\left\{\tau, \gamma_1, \tau\gamma_1, \tau^2\right\} \tag{20}$$

4.4.3 Axial brace loading

Under axial brace loading, relevant chord-side stress concentrations occur at the crown, saddle heel, and saddle toe. The geometrical effects are therefore evaluated separately for the three evaluation paths. Figure 20 shows representative response surfaces for the IIW plate approach [14, 15], with parameters not displayed on the respective axes fixed at their center-point values.

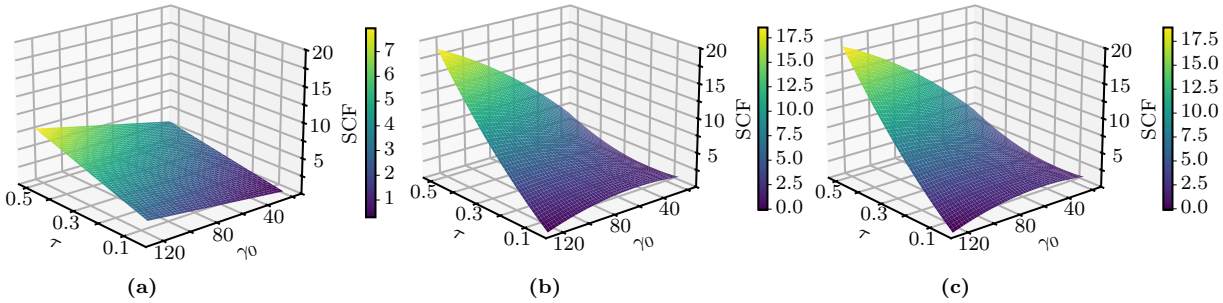


Fig. 20 Axial brace loading, IIW plate approach [14, 15] (a) Crown position, (b) Saddle heel, (c) Saddle toe

At the crown position, τ, γ_0, β, and θ were identified as significant parameters. The retained interaction term $\tau\gamma_0$ indicates that the influence of the thickness ratio depends on the chord slenderness, while the quadratic term β^2 reflects a nonlinear dependence on the diameter ratio. At the saddle heel, the same four parameters were identified as significant, whereas the reduced RSM additionally contains several interaction and quadratic terms, indicating a more pronounced coupled and nonlinear geometrical response. The resulting SCF levels are substantially higher than at the crown position. A similar response is obtained at the saddle toe, for which τ, γ_0, and β are significant, while no statistically significant influence of θ was identified. Overall, the saddle response is characterized by stronger interaction effects between the relative wall-thickness configuration, chord-shell flexibility, and brace-to-chord diameter ratio. The retained RSM terms for the three evaluation paths are summarized in Equations (21) to (23).

$$SCF_{\text{Axial brace loading, Crown,(a)}} = f\left\{\tau, \gamma_0, \tau\gamma_0, \beta^2, \beta, \theta\right\} \tag{21}$$

$$SCF_{\text{Axial brace loading, Saddle heel,(b)}} = f\left\{\tau, \gamma_0, \beta, \tau\gamma_0, \tau\beta, \beta^2, \tau^2, \gamma_0^2, \theta\right\} \tag{22}$$

$$SCF_{\text{Axial brace loading, Saddle toe,(c)}} = f\left\{\tau, \gamma_0, \beta, \tau\gamma_0, \tau\beta, \beta^2, \tau^2, \gamma_0^2\right\} \tag{23}$$

4.4.4 Bending brace loading

For brace bending, the governing hot-spot position depends on the bending direction. Out-of-plane bending of the brace leads to pronounced stress concentrations in the saddle region, whereas the crown position is mainly affected by the in-plane bending configuration. Therefore, the geometrical effects are discussed separately for the relevant evaluation paths. Figure 21 shows representative response surfaces for the IIW plate approach [14, 15].

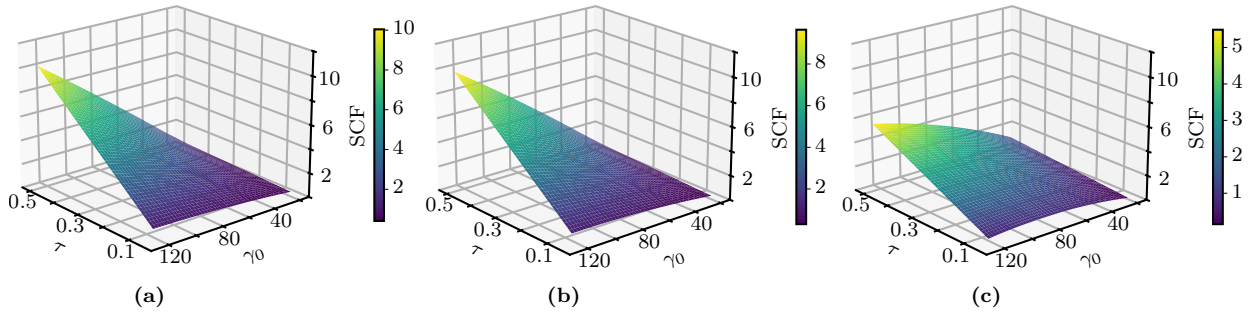


Fig. 21 Bending brace loading, IIW plate approach [14, 15] (a) OPB Saddle heel, (b) OPB Saddle toe, (c) IPB Crown position

For out-of-plane brace bending, the saddle heel and saddle toe exhibit closely comparable parameter dependencies. In both cases, τ, γ_0, and β were identified as significant geometrical parameters. The reduced RSMs additionally retain the interaction products $\tau\gamma_0$, $\tau\beta$, and $\gamma_0\beta$, together with the quadratic terms γ_0^2 and β^2. This indicates that the saddle response under OPB is governed by coupled geometrical effects rather than by independent linear contributions of the individual parameters. In particular, the influence of the relative wall-thickness configuration is dependent on both chord slenderness and diameter ratio, while the quadratic terms account for the nonlinear variation of the SCF with γ_0 and β. The retained RSM terms for the saddle heel and saddle toe are summarized in Equations (24) and (25).

$$SCF_{\text{OPB brace loading, Saddle heel}} = f\left\{\tau, \gamma_0, \beta, \tau\gamma_0, \tau\beta, \gamma_0\beta, \gamma_0^2, \beta^2\right\} \tag{24}$$

$$SCF_{\text{OPB brace loading, Saddle toe}} = f\left\{\tau, \gamma_0, \beta, \tau\gamma_0, \tau\beta, \gamma_0\beta, \gamma_0^2, \beta^2\right\} \tag{25}$$

For in-plane brace bending, the relevant stress concentration occurs at the crown position. In addition to τ, γ_0, and β, the brace inclination θ was identified as a significant parameter. Compared with the OPB cases, the corresponding RSM exhibits a more pronounced dependence on the brace inclination, as reflected by the interaction products $\tau\theta$ and $\beta\theta$ as well as the quadratic term θ^2. Together with the retained products $\tau\gamma_0$, $\tau\beta$, γ_0^2, and β^2, this indicates a coupled nonlinear response involving both the relative brace-chord geometry and the brace orientation. The retained RSM terms for the IPB crown position are summarized in Equation (26).

$$SCF_{\text{IPB brace loading, Crown}} = f\left\{\tau, \gamma_0, \beta, \tau\gamma_0, \tau\beta, \tau\theta, \gamma_0^2, \beta^2, \theta, \beta\theta, \theta^2\right\} \tag{26}$$

5 Discussion

The results demonstrate that the choice of structural stress definition has a systematic influence on the calculated stress concentration for the investigated single-sided welded CHS joints. The magnitude of the method-dependent differences strongly depends on the loading condition, evaluation position, and joint geometry. The largest deviations occur for brace IPB at the crown, while pronounced position-dependent differences are also observed at the saddle. For the surface-extrapolation approaches, these differences can be related to the location of the prescribed reference points relative to the local surface-stress gradient. Owing to the pronounced brace-to-chord scale differences investigated here, the geometry-dependent CHS reference points may be located either comparatively close to the weld toe or further into regions approaching the nominal stress field. Consequently, the different extrapolation procedures sample different portions of the same stress gradient and may therefore yield different structural stresses. This position dependence is consistent with previous observations by Vieira Ávila et al. [13] that the selected HSS evaluation procedure can significantly affect the resulting SCFs in welded tubular joints. The present results further indicate that this sensitivity becomes particularly relevant for geometries with pronounced scale differences outside the conventional CHS applicability ranges. Accordingly, the transferability of established CHS-based reference-point definitions to large-scale monopile

attachments should be verified rather than assumed.

The LEFM-based assessment further indicates that the investigated stress definitions differ in their ability to normalize the geometry-dependent fatigue response. All structural stress approaches substantially reduce the scatter compared with the nominal-stress representation, confirming that the local stress concentration constitutes an essential part of the geometry dependence. The particularly low residual scatter obtained with the XY approach indicates that the stress evaluated 1 mm below the weld toe captures the geometry-dependent stress field governing the adopted crack-growth model with high consistency over the investigated parameter range. In contrast to surface extrapolation, the XY stress is evaluated along the prospective crack path and therefore incorporates the subsurface stress gradient that directly affects crack propagation. A similarly reduced, although larger, scatter was obtained for the Dong structural stress approach. In the implementation used here, the membrane and bending components are derived from the through-thickness normal-stress distribution at the critical cross section. The resulting structural stress therefore retains information on the through-thickness stress field rather than relying exclusively on surface stresses at predefined extrapolation distances. The results show in addition that the design S-N curves of all approaches need to differ since the SCFs between the approaches vary systematically in height. This is especially relevant for the XY approach that results in SCFs larger by a factor of approx. 1.5, see Figure 15.

The identified geometrical sensitivities are broadly consistent with previous investigations of tubular joints, which reported pronounced effects of thickness ratio τ, diameter ratio β, and chord slenderness γ_0 on the resulting SCFs [8, 9]. The present results further demonstrate that the relative importance of these parameters depends strongly on the applied loading mode and evaluation position. In particular, chord loading is predominantly governed by the thickness ratio τ and brace slenderness γ_1, whereas brace loading additionally exhibits pronounced dependencies on chord slenderness γ_0 and diameter ratio β. The retained interaction and quadratic terms indicate that these influences cannot generally be treated as independent linear effects. This becomes particularly relevant for geometries outside the conventional CHS applicability ranges, for which extrapolation of existing parametric SCF formulations may therefore be insufficient.

The numerical models employed an idealized weld geometry derived from the local dihedral angle and an AWS D1.1-oriented weld profile [31]. This provides a consistent basis for the comparative assessment of the investigated stress approaches, but does not represent the variability of the as-built weld geometry. Local deviations in weld toe position, weld angle, convexity, undercuts, misalignment or other geometric imperfections may modify the local stress field and thereby affect the resulting fatigue-relevant stress. Recent work by Brömer et al. [33] demonstrates the potential of incorporating measured three-dimensional weld geometries into the fatigue assessment of tubular joints. Such scan-based models can explicitly account for manufacturing-induced geometric deviations and may therefore provide an improved representation of local eccentricities and stress concentrations. The present idealization should consequently be regarded as a controlled reference geometry, while the influence of as-built weld variability requires separate validation.

The derived SCFs are additionally conditional on the structural system represented in the numerical model. The normalized chord length was fixed at $\alpha = 2$, and the resulting parameter trends therefore apply to the selected chord length and boundary configuration. Variations in chord length or restraint may influence the contribution of chord-shell deformation and secondary bending to the local stress state. The present RSM results should therefore not be extrapolated to different system configurations without additional verification.

The LEFM-based fatigue strength provides an independent computational reference, but remains subject to the assumptions inherent to the adopted crack model, crack-growth formulation and material parameters. The resulting FAT classes are therefore not experimentally calibrated fatigue strengths, but consistently derived reference quantities for comparing the geometry sensitivity of the investigated stress concepts. Accordingly, the reduced scatter obtained for individual structural-stress definitions should be interpreted as improved consistency with the adopted LEFM reference rather than as direct proof of superior fatigue-life prediction. Experimental validation on representative welded joints, ideally including measured as-built weld geometries, remains necessary before transferring the observed trends to design applications.

6 Conclusion

The present study investigated the applicability of different structural stress assessment approaches to single-sided welded tubular joints with pronounced geometric scale differences representative of monopile secondary attachments. Based on the numerical parameter study and the LEFM-based reference assessment, the following conclusions are:

- The XY approach showed the strongest consistency with the geometry-dependent fatigue response predicted by LEFM. A coefficient of determination of $R^2 = 0.999$ was obtained between the calculated SCFs and the LEFM-derived nominal FAT classes. After transformation to the corresponding structural-stress level, the scatter was reduced to $T_\sigma = 1.07$, representing the lowest scatter among all investigated stress approaches. The Dong approach likewise showed a comparatively high consistency ($R^2 = 0.980$, $T_\sigma = 1.33$), whereas the conventional surface-extrapolation approaches according to IIW, IIW/CIDECT and DNV resulted in larger remaining scatter, with T_σ between 1.51 and 1.66.
- The investigated stress approaches show method-dependent differences that vary with loading condition, evaluation position, and joint geometry. The largest deviations were observed for brace IPB at the crown, while position-dependent differences were also evident at the saddle locations. For the surface-extrapolation methods, the location of the prescribed reference points relative to the local stress gradient represents an important source of these deviations.
- The geometrical parameter dependencies are strongly load-case dependent. For chord loading, the SCF is significantly influenced by the thickness ratio τ and the brace slenderness γ_1, with the relevant stress concentration occurring at the crown position. For brace loading, τ, the chord slenderness γ_0, and the diameter ratio β consistently exhibit significant influences, while the brace inclination θ becomes

relevant for selected loading conditions and evaluation paths. The retained interaction and quadratic terms demonstrate that the SCF response, particularly for brace loading, cannot generally be represented by independent linear parameter effects.

- The relevant hot-spot position depends on the loading mode. Axial brace loading produces relevant stress concentrations at both crown and saddle positions, whereas OPB primarily affects the saddle region and IPB the crown region.
- The combined DoE–RSM framework enabled the identification of load-case-specific geometrical sensitivities, interaction effects, and nonlinear effects within the investigated parameter domain.

The conclusions are conditional on the modeling assumptions adopted in this study, including the idealized AWS-oriented weld geometry, the fixed normalized chord length, the selected boundary conditions, and the assumptions inherent in the analytical LEFM reference. Experimental validation is required before transferring the observed trends to fatigue design practice.

Acknowledgments

The authors gratefully acknowledge IPU Ingenieurgesellschaft Braunschweig mbH (Germany), for their collaboration and valuable contributions to the research project.

Declaration of Generative AI and AI-assisted technologies in the writing process

During the preparation of this work the authors used ChatGPT (based on GPT-5.5 OpenAI) in order to reorganize the notes and improve the manuscript readability. After using this tool/service, the authors reviewed and edited the content as needed and take full responsibility for the content of the published article.

Statements and Declarations

Funding

The research project "Verbesserung der Lebensdauerbewertung einseitig geschweißter T-Knoten aus dickwandigen Hohlprofilen bei Offshore-Gründungsstrukturen" is funded by the Federal Ministry of Economic Affairs and Climate Action as part of the "Industrial Collective Research" program on the basis of a resolution of the German Bundestag. This project 01IF23538N / P1704 from the Research Association for steel Application (FOSTA), Düsseldorf, is carried out at the Institute of Steel Structures, TU Braunschweig.

Competing interests

The authors declare that they have no conflict of interest.

Data availability

The data can be accessed under doi: 10.5281/zenodo.23345009, see [34].

Code availability

The code developed for this study is available from the corresponding author upon request.

Ethics approval and consent to participate

Not applicable.

Consent for publication

Not applicable.

Author contributions

S. Vogts: Conceptualization, Methodology, Visualization, Investigation, Formal analysis, Data curation, Writing – original draft. **J. Baumgartner**: Methodology, Data curation, Validation, Investigation, Writing – review & editing. **J. Unglaub**: Project administration, Funding acquisition, Supervision, Writing – review & editing. **K. Thiele**: Funding acquisition, Supervision, Resources, Writing – review & editing.

References

[1] Liang, R., Yuan, Y., Fu, D., Liu, R.: Cyclic response of monopile-supported offshore wind turbines under wind and wave loading in sand. Marine Georesources & Geotechnology **39**(10), 1230–1243 (2021) https://doi.org/10.1080/1064119X.2020.1821848

[2] Rezaei, R., Fromme, P., Duffour, P.: Fatigue life sensitivity of monopile-supported offshore wind turbines to damping. Renewable Energy **123**, 450–459 (2018) https://doi.org/10.1016/j.renene.2018.02.086

[3] Albiez, M., Boretzki, J., Ummenhofer, T.: Adhesive bonding of secondary steel components for offshore wind turbines. ce/papers **6**(3-4), 959–963 (2023) https://doi.org/10.1002/cepa.2650

[4] Jungen, J.-W., Lochte–Holtgreven, S.: On local stress distributions in impact–loaded offshore steel substructures. ce/papers **9**(2-3), 2826–2830 (2026) https://doi.org/10.1002/cepa.70736

[5] Saini, D.S., Karmakar, D., Ray-Chaudhuri, S.: A review of stress concentration factors in tubular and non-tubular joints for design of offshore installations. Journal of Ocean Engineering and Science **1**(3), 186–202 (2016) https://doi.org/10.1016/j.joes.2016.06.006

[6] Zavvar, E., Rosa-Santos, P., Taveira-Pinto, F., Ghafoori, E.: Lifetime extension of offshore support structures of wind turbines: A review. Renewable and Sustainable Energy Reviews **217**, 115788 (2025) https://doi.org/10.1016/j.rser.2025.115788

[7] Atteya, M., Mikkelsen, O., Wintle, J., Ersdal, G.: Experimental and numerical study of the elastic scf of tubular joints. Materials (Basel, Switzerland) **14**(15) (2021) https://doi.org/10.3390/ma14154220

[8] Yang, Y., Min, S., Peng, Y., Wang, H., Chen, C.: Experimental and numerical investigation on stress concentration factor of large-scale welded tubular t-joints. Ocean Engineering **320**, 120337 (2025) https://doi.org/10.1016/j.oceaneng.2025.120337

[9] Zavvar, E., Ehlers, S., Rosa Santos, P.: Maximum stress concentration factors in dkt joints subjected to combined compression and tension loads. Ships and Offshore Structures, 1–12 (2025) https://doi.org/10.1080/17445302.2025.2453668

[10] Liang, G., Hou, C., Tan, Q.: Probability model for scf in cfst joints under axial loading and in-plane bending. Journal of Constructional Steel Research **217**, 108660 (2024) https://doi.org/10.1016/j.jcsr.2024.108660

[11] Iqbal, M., Karuppanan, S., Perumal, V., Ovinis, M., Nouman, H.: Empirical modeling of stress concentration factors using finite element analysis and artificial neural networks for the fatigue design of tubular kt–joints under combined loading. Fatigue & Fracture of Engineering Materials & Structures **46**(11), 4333–4349 (2023) https://doi.org/10.1111/ffe.14122

[12] Vogts, S., Unglaub, J., Thiele, K.: Numerical study of hot–spot stresses in single sided welded t–joints for fatigue assessment of offshore foundations. ce/papers **9**(2-3), 2820–2825 (2026) https://doi.org/10.1002/cepa.70642

[13] Vieira Ávila, B., Correia, J., Carvalho, H., Fantuzzi, N., Jesus, A., Berto, F.: Numerical analysis and discussion on the hot-spot stress concept applied to welded tubular kt joints. Engineering Failure Analysis **135**, 106092 (2022) https://doi.org/10.1016/j.engfailanal.2022.106092

[14] Niemi, E., Fricke, W., Maddox, S.J.: Structural Hot-Spot Stress Approach to Fatigue Analysis of Welded Components. Springer Singapore, Singapore (2018). https://doi.org/10.1007/978-981-10-5568-3

[15] Hobbacher, A.F., Baumgartner, J.: Recommendations for Fatigue Design of Welded Joints and Components. Springer Nature Switzerland, Cham (2024). https://doi.org/10.1007/978-3-031-57667-6

[16] DNV AS: Fatigue design of offshore steel structures (DNV-RP-C203) (2024).

Edition October 2024

[17] Machač, M., Papuga, J., Doubrava, K., Barsoum, Z., Yıldırım, H.C.: Fatigue behaviour and thickness effect in thin-walled welded hollow section joints: evaluation using hot-spot stress approach. International Journal of fatigue **208**, 109565 (2026) https://doi.org/10.1016/j.ijfatigue.2026.109565

[18] Zhao, X.-L., Packer, J.A.: Fatigue Design Procedure for Welded Hollow Section Joints: IIW Document XIII-1804-99 and IIW Document XV-1035-99 : Recommendations of IIW Subcommission XV-E. Woodhead Publishing Series in Welding and Other Joining Technologies. Abington Pub, Cambridge, England (2000). https://doi.org/10.1533/9780857093127

[19] Zhao, X.-L., Herion, S., Packer, J.A., Puthli, R.S., Sedlacek, G., Wardenier, J., Weynand, K., van Wingerde, A.M., Yeomans, N.F. (eds.): Design Guide for Circular and Rectangular Hollow Section Welded Joints Under Fatigue Loading. Construction with hollow steel sections, vol. 8. TÜV-Verl., Köln (2001)

[20] Xiao, Z.-G., Yamada, K.: A method of determining geometric stress for fatigue strength evaluation of steel welded joints. International Journal of fatigue **26**(12), 1277–1293 (2004) https://doi.org/10.1016/j.ijfatigue.2004.05.001

[21] Dong, P.: A structural stress definition and numerical implementation for fatigue analysis of welded joints. International Journal of fatigue **23**(10), 865–876 (2001) https://doi.org/10.1016/S0142-1123(01)00055-X

[22] Williamson, E.M., Sun, Z., Mora-Tamez, L., Brutchey, R.L.: Design of experiments for nanocrystal syntheses: A how-to guide for proper implementation. Chemistry of Materials **34**(22), 9823–9835 (2022) https://doi.org/10.1021/acs.chemmater.2c02924

[23] Kremer, A.: Statistische versuchsplanung in der lebensdauererprobung mit vertrauensintervallen. Dissertation, Universität Stuttgart (2021). https://elib.uni-stuttgart.de/server/api/core/bitstreams/0d8deefd-a5ef-4f82-ae72-bf34aafaf450/content

[24] Shen, G., Plumtree, A., Glinka, G.: Weight function for the surface point of semi-elliptical surface crack in a finite thickness plate. Engineering Fracture Mechanics **40**(1), 167–176 (1991) https://doi.org/10.1016/0013-7944(91)90136-O

[25] Dong, P., Hong, K.J., Osage, D.A., Dewees, D.J., Prager, M.: The master S-N curve method: An implementation for fatigue evaluation of welded components in the ASME B&PV code, Section VIII, Division 2 and API 579-1/ASME FFS-1. Technical Report WRC Bulletin 523, Welding Research Council (2010)

[26] American Society of Mechanical Engineers: ASME Boiler and Pressure Vessel

Code, Section VIII: Rules for Construction of Pressure Vessels, Division 2: Alternative Rules. American Society of Mechanical Engineers, New York (2019). ASME BPVC.VIII.2-2019

[27] American Petroleum Institute, American Society of Mechanical Engineers: API 579-1/ASME FFS-1: Fitness-For-Service. American Petroleum Institute, Washington, DC (2016). Third Edition

[28] Paris, P.C., Erdogan, F.: A critical analysis of crack propagation laws. Journal of Basic Engineering **85**(4), 528–533 (1963) https://doi.org/10.1115/1.3656900

[29] Müller, D., Stöber, M., Thümmler, A.: Einsatz der Response-surface-Methode zur Optimierung komplexer Simulationsmodelle. Technische Universität Dortmund. (2005) https://doi.org/10.17877/DE290R-7704

[30] Oliveira, L.G., Paiva, A.P., Balestrassi, P.P., Ferreira, J.R., Da Costa, S.C., Da Silva Campos, P.H.: Response surface methodology for advanced manufacturing technology optimization: theoretical fundamentals, practical guidelines, and survey literature review. The International Journal of Advanced Manufacturing Technology **104**(5-8), 1785–1837 (2019) https://doi.org/10.1007/s00170-019-03809-9

[31] American Welding Society: AWS D1.1/D1.1M:2020 Structural Welding Code—Steel, 24 edn. American Welding Society, Miami, FL (2020)

[32] Hectors, K., De Waele, W.: Influence of weld geometry on stress concentration factor distributions in tubular joints. Journal of Constructional Steel Research **176**, 106376 (2021) https://doi.org/10.1016/j.jcsr.2020.106376

[33] Brömer, T., Widerspan, V., Shojai, S., Ghafoori, E.: Enhanced local fatigue approach for welded tubular joints using 3d digital scans and implicit gradient model. International Journal of fatigue **199**, 109060 (2025) https://doi.org/10.1016/j.ijfatigue.2025.109060

[34] Vogts, S.: Dataset to "LEFM-Based Evaluation of Structural Stress Approaches for Fatigue Assessment of Welded CHS with Large Geometric Scale Differences". Zenodo (2026). https://doi.org/10.5281/zenodo.23345009